International Journal of Heat and Mass Transfer 70 (2014) 578–585

Contents lists available at ScienceDirect

International Journal of Heat and Mass Transfer

journal homepage: www.elsevier.com/locate/ijhmt

Experimental analysis of low air pressure influences on fire plumes

Zhihui Zhou [a,c], Yao Wei [b], Haihang Li [a], Richard Yuen [c], Wang Jian [a,*]

[a] State Key Laboratory of Fire Science, University of Science and Technology of China, Hefei 230027, PR China
[b] LHD, Institute of Mechanics, Chinese Academy of Sciences, Beijing 100190, PR China
[c] Department of Civil and Architectural Engineering, City University of Hong Kong, Hong Kong 999077, PR China

ARTICLE INFO

Article history:
Received 8 July 2013
Received in revised form 31 October 2013
Accepted 13 November 2013
Available online 8 December 2013

Keywords:
Low air pressure
Burning rate
Dimensionless heat release
Fire plume

ABSTRACT

To examine the pressure effect on burning rate, flame height and axial temperature distribution of diffusion fires, experimental measurement and theoretical analysis on circular n-Heptane fires with serial sizes were conducted at two altitudes, i.e. 100.8 kPa (in a sea-level city Hefei) and 64.3 kPa (in a Tibetan city Lhasa). From the results, the mean burning rate at quasi-steady stage and boiling stage consistently implied that the exponent α ($\dot{m}'' \underset{D}{\sim} P^{\alpha}$) varies for different heat transfer domination stages, i.e. $\alpha \leqslant 0$ for conductive stage and $\alpha = 2/3$ for convective stage. Analysis shows that the flame height, the axial flame and plume temperatures are all well correlated with the dimensionless heat release rate $Q^* \sim Q/(PD^{5/2})$, with the correlation coefficients derived from the current low-pressure measurements. Analysis shows that the flame height and the plume temperature increase with the pressure rise as a power function of pressure for the same pool size.

Contents

1. Introduction

Altitude tests have confirmed that low air pressure plays significant effects on mass burning rate ($\dot{m}$), or fire load Q. Earlier European standard EN54 fire tests at four altitudes between 420 and 3000 m (97–71 kPa) pointed out that mass transfer flux $\dot{m}'' \underset{D}{\sim} P^{\alpha}$ (the symbol $\underset{D}{\sim}$ denotes the proportional relationship for the same burner size D), with P the pressure and $\alpha \approx 1.3$ [1]. Since the building of a high-altitude fire in Lhasa (3658 m/64.3 kPa) of Tibet, a series of fire tests with different experimental parameters have been conducted. Li et al. [2] firstly reported the experimental results on n-Heptane and wood crib fires in Hefei (50 m/100.8 kPa) and Lhasa, and verified the correlation obtained by Wiser et al. [1]. Hu et al. [3] conducted n-Heptane fire tests in Dangxiong (4350 m/5.91 kPa) and Lhasa, and suggested that $\dot{m}'' \sim fcn\,(D, P)$, with D the pool diameter. Fang et al. [4,5] summarized the data from square pool fires with different sizes (D = 4–33 cm), and obtained $\dot{m}'' \underset{D}{\sim} P^{\alpha}$, where α is related to the flame heat feedback terms. Rectangular ethanol and n-Heptane fires tested in Hefei and Lhasa by Tu et al. [6] indicated that $\dot{m}'' \underset{D}{\sim} P$ under radiation-controlled condition. Cardboard box fires of different sizes specified by federal aviation administration (FAA) minimum performance standard (MPS) [7] were tested in Hefei and Lhasa by Niu and Yao et al. [8,9], where it is found that mass burning rate and radiative heat flux decrease while plume temperature increases under lower pressure.

* Corresponding author. Tel.: +86 551 63606463; fax: +86 551 6360643.
E-mail address: wangj@ustc.edu.cn (W. Jian).

0017-9310/$ - see front matter © 2013 Elsevier Ltd. All rights reserved.
http://dx.doi.org/10.1016/j.ijheatmasstransfer.2013.11.042

Nomenclature

A_f	flame surface area (m^2)
c_p	specific heat (J/kg K)
D	burner diameter (m)
f_v	soot volume fraction
g	acceleration of gravity (m/s^2)
h	heat transfer coefficient (k W/m^2 K)
H_c	heat of combustion (kJ/g)
k	thermal conductivity (k W/m K)
$\dot{m}$	burning rate (g/s)
$\dot{m}''$	burning intensity (g/m^2 s)
L_m	mean bean length (m)
R_l	fuel regression rate (m/s)
P	ambient pressure (kPa)
Q	heat release rate (kW)
Q^*	dimensionless heat release rate (–)
$\dot{q}''$	Heat flux (k W/m^2)
r	stoichiometric mass rate, air to fuel (–)
t	time (s)
T	temperature (K)
T_s	fuel surface temperature (K)
X_r	radiant fraction (–)
V_f	flame volume (m^3)
z	axial height (m)
z^*	characteristic flame length (–)
z_0	virtual origin (m)
z_f	flame height (m)
κ	effective absorption coefficient (m^{-1})
ρ_∞	air density (kg/m^3)
σ	Stefan–Boltzmann constant ($W/m^2 K^4$)

Subscripts

f	flame
h	Hefei
l	Lhasa
r	radiative
s	liquid surface
st	quasi-steady phase
bl	boiling phase
∞	ambient

Theoretical modeling approach has been used to correlate the fire plume parameters with total heat release rate Q and pool size D based on experimental data at standard pressure. Thomas [10] derived a dimensionless relationship for flame height, i.e. $z_f/D \sim fcn\,(Q^2/gD^5)$. McCaffrey [11] identified the three distinct regimes by the correlations of axial velocity and axial temperature with scaled axial height in a buoyant methane diffusion flame on a 0.3 m square porous burner. Zukoski introduced the concept of dimensionless heat release rate ($Q^* = Q/(\rho_\infty c_p T_\infty \sqrt{g} D^{5/2})$) and dimensionless flame height to describe diffusion flames and plumes in a unified way [12,13]. A model for correlating measurements of virtual origins for finite axisymmetric sources was proposed by Heskestad, with which mean flame height can be well predicted [14–17]. Quintiere formulated the behavior of fire plumes by a set of unified correlations, which included another important factor, radiation fraction (X_r) [18].

Fang et al. recorded the change in the axial temperature with $z/Q^{2/5}$ for n-Heptane and ethanol fires at high altitude, without consideration of the varied air density aroused by pressure [4]. Yin et al. investigated the altitude influence on small pool fires with a pressure chamber of 3 m × 2 m × 2 m, and pointed out the importance of low air pressure influence on Q^*, as $Q^* \underset{D}{\sim} Q/\rho_\infty \underset{D}{\sim} Q/P$, with which the dimensionless fire plume temperature ($(T - T_\infty)/T_\infty$) is correlated with the pressure to the power of −2/3 [19].

In order to unify the air pressure influences on fire plumes, a series of circular pool fires with different sizes were tested in Hefei and Lhasa. The combustion characteristics of fire plumes, such as mass burning rate, flame height and axial temperature distribution were measured to establish a unified analysis of air pressure influences upon fire plume. The classical theoretical modelings and their simplified forms will be discussed and compared to verify their applicability under low air pressure.

2. Experimental setup

The experiments were conducted in Hefei and Lhasa, respectively under the condition of similar ambient temperatures and humidities (Hefei: 15 ± 2 °C, 45% ± 5%; Lhasa: 15 ± 3 °C, 40% ± 4%). Fig. 1 shows the schematic diagram of experimental setup.

Five different sizes of circular pans were adopted, with the diameters of 6, 8, 10, 12, and 14 cm, respectively. The burners were constructed by steel, with 2 cm in depth and 0.32 ± 0.01 cm in thickness. Electronic scale (METTLER TOLEDO, XP 10002S) with the resolution of 0.1 g was used to record the mass loss of fuel during burning. A 30 cm × 30 cm insulation board was placed on the top of scale to shield the high temperature. To minimize the effect of soot deposition on temperature measurement, the thinner K-type armored thermocouples with diameter of 0.5 mm [19] and response time less than 1 s were adopted. An array of 14 thermocouples was located vertically along the axis of the burner. The lower eight thermocouples were spaced 5 cm between each other, and the upper six ones were spaced 10 cm. The temperature measurements reported in this study were the direct thermocouple readings without radiation correction which may yield an uncertainty less than 10% [20] depending largely on the level of soot radiation. The boiling of liquid fuel was monitored by a high-resolution CCD camera. Another 25-fps video camera (Sony, HDR-XR160E) was place 1.5 m away from the fire axis to record flame images.

In the experiments, n-Heptane was selected as the tested fuel with industrial purity above 99% (impurity contents: volatile ⩽0.05%, water ⩽0.05%, unsaturated compounds in Br+ ⩽0.032%),

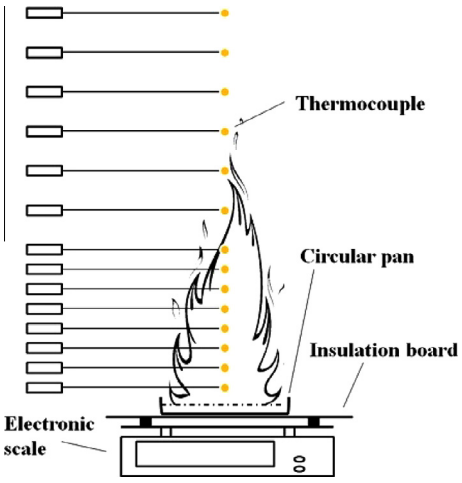

Fig. 1. Schematic diagram of experimental setup.

Table 1
Summary of fire tests.

Fuel	Location	Pressure (kPa)	Diameter of burners (cm)	Measurement
n-Heptane[a] (C_7H_{16})	Hefei Lhasa	98.6 64.3	6, 8, 10, 12, 14	(1) Mass loss (2) Temperature (3) Video record

[a] Parameters for liquid n-Heptane: density 679.5 kg/m^3, latent heat 318 kJ/kg, enthalpy of combustion 48.5 MJ/kg.

whose density is 683–685 kg/m^3, boiling range is 96.5–98.5 °C, self-ignition temperature is 223.0 °C and the explosion limits is 1.05–6.7% [4,19]. n-Heptane was filled into the burner to a height of 1.5 cm, equivalent to 28.8, 51.2, 80.1, 115.3, and 156.9 g for the pools from the smallest to the largest. Summary of fire tests was listed in Table 1, where tests of the same configuration were repeated for at least three times to ensure the repeatability.

3. Results and discussion

Compared with pool fire with infinite depth, the thin-layer fuel burning process is more complicated since boiling phenomenon is involved, especially for n-Heptane with a lower boiling point [21]. Due to the enhanced thermal effects from the vessel wall and bottom, the burning fuel is prone to bubble up [21]. Four typical phases namely pre-burning stage (I), quasi-burning stage (II), boiling–burning stage (III) and decay stage (IV) were identified by Kang et al. [21], which were also observed in the current tests. Fig. 2 plots the variation of burning rate and flame height in the entire burning process for the 14 cm pool fires. The quasi-steady burning stage occurs after a short pre-burning, and continues for about 350 and 450 s in Hefei and Lhasa tests, respectively. In the quasi-steady stage, the burning rate and flame height increase at approximately the constant rates. In the boiling stage, the increase in burning rate suddenly accelerates and leads to a quick development of fire. As predicted by $z_f \sim (Q^*)^{2/5} \underset{D}{\sim} (\dot{m})^{2/5}$ at a fixed pressure, the change in flame height is not as much as that in mass burning rate, which can be seen from Fig. 2 that the burning rate peaks occur at certain range where the flame height seem not changing much. From the video records of fuel surface, as shown in Fig. 3, the boiling stage starts with some bubbles emerging around the vessel rim when the fuel is consumed to about 0.48 cm high, then the bubbles rapidly accumulates on the fuel surface. The generation of bubbles on the solid–liquid interface is so called nucleate boiling phenomenon, which can significantly promote the heat exchange between the wall and the fuel, and lead to a rapid growth in the burning rate [21]. When the fuel level decreases to 0.19 cm, the fuel has already fully boiled. The flame height continues to increase in the boiling stage, but the increment of flame height is much less sensitive to the boiling than that of burning rate. From the experimental observation, the burning rate decreases under low pressure, but the flame height increases distinctly. The averaged burning intensities (burning rate per unit area) and flame heights in quasi-steady burning stage and boiling stage for tests in Hefei and Lhasa were calculated in Table 2, denoted by $\dot{m}''_{h,st}, \dot{m}''_{h,bl}, \dot{m}''_{l,st}, \dot{m}''_{l,bl}, z_{fh,st}, z_{fh,bl}, z_{fl,st}, z_{fl,bl}$ respectively, where h and l represent Hefei and Lhasa, bl and st represent boiling and quasi-steady burning.

3.1. Mass loss

Previous studies [4,22,23] indicated that burning intensity is mainly determined by the heat transfer from flame to fuel surface through conduction, convection and radiation,

$$\dot{m}'' \sim 4\frac{k(T_f - T_s)}{D} + h(T_f - T_s) + \sigma(T_f^4 - T_s^4)(1 - \exp(-\kappa L_m)) \quad (1)$$

where T_f is the flame temperature near the burner surface, and will increase slightly under low air pressure [2,4]; T_s is the fuel surface temperature, and is usually regarded as fuel boiling temperature [21,23], i.e. 98.5 °C in Hefei and 89 °C in Lhasa for n-Heptane in this study [4]. The investigation on the fuel regression rate ($R_l = \dot{m}''/\rho_l$,with ρ_l liquid density) shows that the conduction dominates when the burner diameter D is less than 7 cm, the transition occurs at 7–10 cm, and convection dominates when 10 cm < D < 20 cm [23].

The burning intensity under low pressure can be determined by examining the pressure effects on the three heat feedback terms individually. As suggested by Fang et al. [4,6], the burning intensities vary with pressure as $\dot{m}'' \sim P^{\alpha}$. For the conductive term, it has $\dot{m}'' \sim 4k(T_f - T_s)/D \underset{D}{\sim} P^0$, where the thermal conductivity k is considered as a pressure independent constant. As the low pressure arouse a slight increase in T_f and decrease in T_s, the burning intensity increases slightly due to the conductive term under lower pressure, implying that the exponential parameter α should be a small negative value [4]. For convective term [24], it has $\dot{m}'' \sim h(T_f - T_s)$, where the convective coefficient h decreases with pressure as $h \sim (Gr)^{1/3}(\mathrm{Pr})^{1/3} \sim P^{2/3}$ [24], i.e. $\dot{m}'' \underset{D}{\sim} P^{2/3}$. The variation of exponential factor α was shown in Fig. 4, where three regions are divided by the former analysis on heat feedback terms: I – conductively dominated region ($\alpha < 0$), II – transition region ($0 < \alpha < 2/3$), and III – convectively dominated region ($\alpha \geqslant 2/3$). Fig. 4 shows that α increases with the increasing of burner

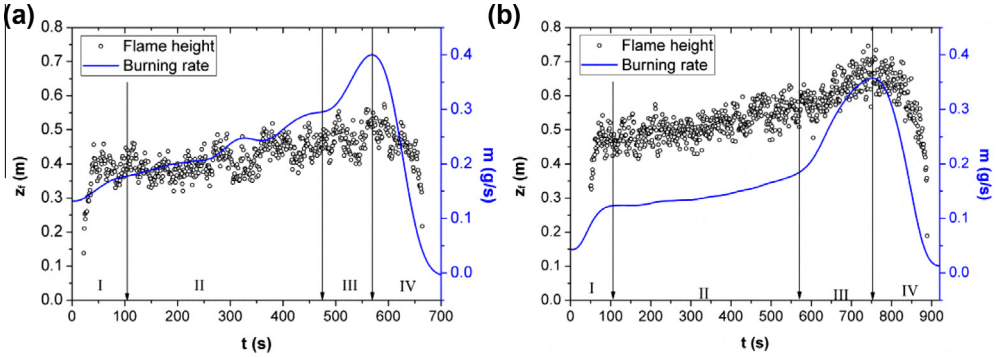

Fig. 2. Flame height and burning rate of 14 cm pool fires (a) in Hefei, and (b) in Lhasa.

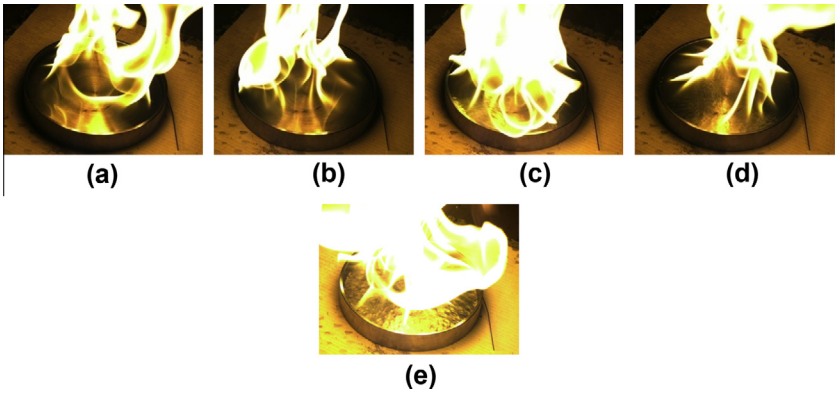

Fig. 3. Image records of fuel surface (a)–(e) corresponding to the fuel level heights of 1.34, 1.05, 0.76, 0.48, and 0.19 cm.

Table 2
The averaged burning intensities and flame heights in Hefei and Lhasa.

D (cm)	$\dot{m}''_{h,st}$ (g/s)	$\dot{m}''_{h,bl}$ (g/s)	$\dot{m}''_{l,st}$ (g/s)	$\dot{m}''_{l,bl}$ (g/s)	$z_{fh,st}$ (cm)	$z_{fh,bl}$ (cm)	$z_{fl,st}$ (cm)	$z_{fl,bl}$ (cm)
6	0.025	0.044	0.023	0.052	22.3	29.1	24.2	35.5
8	0.049	0.083	0.042	0.085	29.7	34.9	30.4	39.8
10	0.083	0.110	0.067	0.118	33.7	40.0	39.1	46.9
12	0.123	0.223	0.104	0.198	39.6	46.8	44.5	54.3
14	0.219	0.357	0.144	0.294	43.4	49.3	51.5	61.7

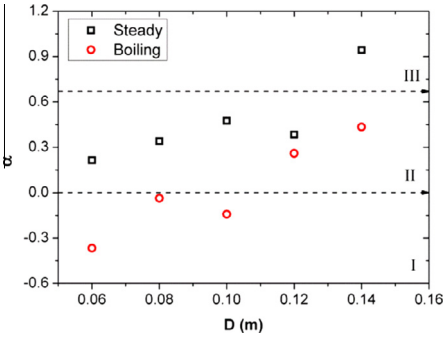

Fig. 4. Exponential factor α for different sizes of burner.

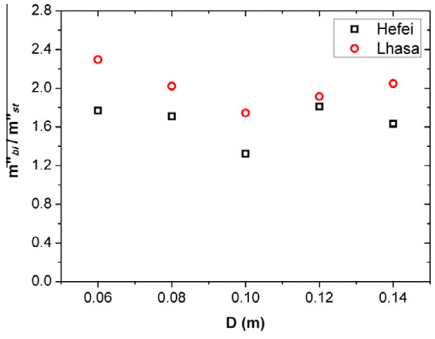

Fig. 5. Variation of $\dot{m}''_{bl}/\dot{m}''_{st}$ in Hefei and Lhasa.

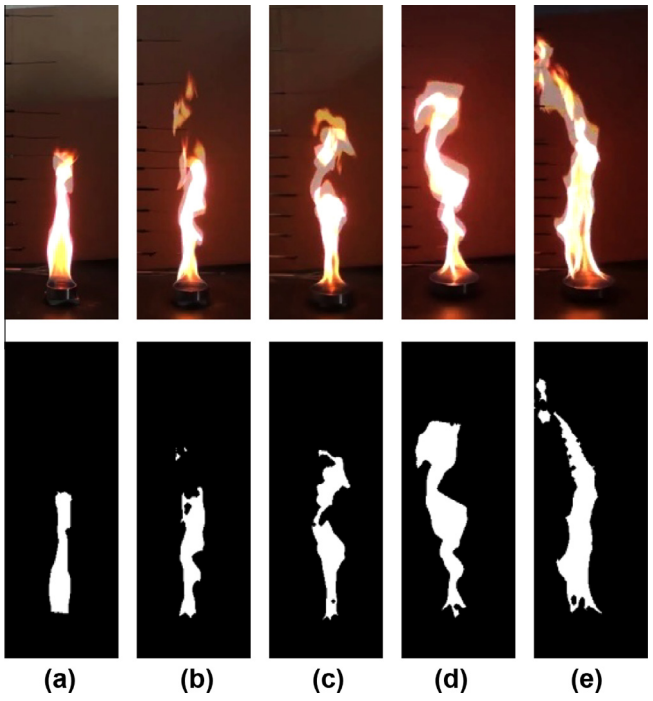

Fig. 6. Flame shapes and their binary images in Lhasa (a)–(e) for 6–14 cm burners at 7500th frame (300.00 s) after the fire ignition.

diameter, which is consistent with the previous report [4]. Generally, the transition from conductively dominated to convectively dominated starts from the pool dimension of around 10 cm. The burning in the boiling stage is more prone to be conductively dominated [21], as also observed in Fig. 4.

Fig. 5 shows the pressure effect on the ratio of $\dot{m}''_{bl}/\dot{m}''_{st}$. The boiling burning relative to steady burning in Lhasa is more violent than in Hefei, which can be attributed to the improved conductive heat transfer caused by the higher flame temperature and lower boiling point under low pressure.

3.2. Flame height

Fig. 6 shows instantaneous flame shapes for different sizes of burner and their corresponding binary images at the 7500th frame (300 s) after the fire ignition. The predicted puffing frequency equaling to $1.5D^{-1/2}$ [25] and the experimental results from Fang

et al. [4] both indicated that flame oscillation frequency should be within the range of 4–9, thus the current image recording speed is acceptable. The RGB images of the entire burning procedure recorded by the Sony camera were firstly converted to binary images. The binary image processing technique used by Hu et al. [3] and Yang et al. [26] was employed to process the 25 fps videos to obtain the flame heights as the time-averaged visible flame heights for the quasi-steady and boiling burning stages, respectively.

The flame height is closely related to the air entrainment. Ideally, the flame should extend to a height (z_f) where the total flux of air entrained along the height is sufficient to consume the fuel [23]. For turbulent flames, excessive entrainment occurs and can reach n times ($n \approx 9.6$) of the air needed for the combustion [18]. A flame height correlation of $z_f/D \sim fcn(Q^*)$ with dimensionless heat release rate was suggested for turbulent flames by previous studies [13,16,17]. The lower ambient pressure indicates a decreasing air density, which reduces the mass flux of air entrainment per unit length and thus the flame requires longer entrainment path, i.e. the flame height to fulfill the combustion.

Zukoski et al. [13] divided the flame into two regions by correlating the flame height z_f with the dimensionless heat release rate Q^*,

$$Q^* < 1, \quad z_f/D = 3.30 \cdot (Q^*)^{2/3} \tag{2}$$

$$Q^* \geqslant 1, \quad z_f/D = 3.30 \cdot (Q^*)^{2/5} \tag{3}$$

Heskestad [16,17] provided a further explicit equation for flame height, which covers the entire diffusion regime of Q^* ($0.12 < Q^* < 1.2 \times 10^4$) [11,23,27,28]

$$z_f/D + 1.02 = 15.6\left(\frac{rC_pT_\infty}{H_c}\right)^{3/5}(Q^*)^{2/5} \tag{4}$$

where, H_c/r is the heat liberated per unit mass of air entering the combustion reactions and is considered pressure independent. For a large number of gaseous and liquid fuels, H_c/r varies slightly [16,23] in the range from 2900 to 3200 kJ/kg [27]. The factor $15.6(rC_pT_\infty/H_c)^{3/5}$ was given as 3.7 in [27].

Fig. 7 shows that the linear fitting results of the measured flame height by method of least squares, which indicates that the dimensionless flame height is highly correlated to the power of dimensionless heat release rate, i.e. $z_f/D \sim (Q^*)^{2/5}$, with Pearson correlation coefficient [29] of $R = 0.89$. Adjusted coefficient of determination $\bar{R}^2$ was introduced to explain the errors in the linear fits [30,31]. The fitted slopes, 3.20 based on Eq. (3) and 3.98 for using Eq. (4) have the adjusted coefficients of determination $\bar{R}^2$ equaling 0.983 and 0.995, respectively, which indicate good agreements with the theoretical predictions, i.e. 3.3 and 3.7.

Furthermore, since Q^* can be scaled by pressure as $Q^* \sim Q/(PD^{5/2}) \underset{D}{\sim} P^{(\alpha-1)}$, then it has $z_f \underset{D}{\sim} P^{0.4(\alpha-1)}$. The exponential factor α is less than 1 as indicated from the above analysis on burning intensity, therefore the flame height increases under low pressure as indicated from the experimental measurements in Table 2. As pressure descends, the air entrainment (denoted by ambient density $\rho_\infty \sim P$) decreases relative to the fuel consumption rate ($\dot{m}'' \underset{D}{\sim} P^\alpha$), then correspondingly the flame will shift to a higher axial position to obtain sufficient oxygen, exhibiting as the stretched visual flame and an increasing in flame height under lower pressure for the same burner size.

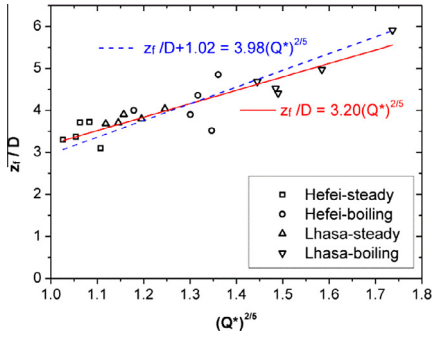

Fig. 7. Averaged flame heights fitted using Zukoski relation [13] and Heskestad relation [16,17].

3.3. Soot and flame radiation

Soot is actually pointed out to be the main contributor of flame radiation for most moderately-sooting (e.g. n-Heptane [32]) and heavily-sooting (e.g. toluene [32]) flames [33]. Previous studies conducted at elevated pressure indicated that soot concentrations show a significant increase with pressure, and generally the pressure dependence of soot can be simplified in the form of a power law dependence. Different fuels show different sensitivities to pressure, and thus, their power law fitting exhibits different scaling factors [34], e.g. a comparison of the pressure dependencies of the soot yield indicates that n-Heptane fueled flame seems to be slightly more sensitive to pressure than both ethane and propane fueled flames, with a power about 2–2.5 [35]. Yao et al. developed a global soot model for fires [36,37] where $f_v \sim P^2$, which had been validated and applied in the modeling of liquid n-Heptane pool fires [38] based on experiments conducted at Lhasa [3]. The square dependence of pressure also coincides with the results in radiation fire modeling proposed by De ris as [39] $\kappa \sim f_v \sim P^2$, where κ is the soot absorption coefficient.

The incident flame heat flux is given as [40]

$$\dot{q}_r'' = \sigma T_f^4[1 - \exp(-\kappa L_m)] \tag{5}$$

where κL_m can be legitimately assumed as a small value, especially under low pressure where soot production is even lower. Thus

$$\dot{q}_r'' \approx \sigma\kappa L_m T_f^4 \sim P^2 L_m T_f^4 \tag{6}$$

where the beam length L_m is given with an optimal factor 3.6, and conventionally expressed as $L_m = 3.6V_f/A_f$ [40,41], thus the flame total radiation can be correlated by $\dot{Q}_r = A_f\sigma\kappa L_m T_f^4 \sim P^2 V_f T_f^4$.

To further evaluate the mean beam length, flame shape is assumed for simplicity a cylinder of diameter D_f and height z_f. On account of $z_f \gg D_f$, L_m can be simplified as [42],

$$L_m = 0.9\left(\frac{z_f/D_f}{z_f/D_f + 1/2}\right)D_f \approx 0.9D_f \tag{7}$$

Combined with Eq. (6), it is logical to express the flame radiative heating on liquid surface by $\dot{q}_{rs}'' \sim P^2 D_f(T_f^4 - T_s^4)$, which is proportional to burning intensity $\dot{m}''$ under the radiation domination. It is well agreed with the experimental results, $\dot{m}'' \sim P^\alpha$ ($\alpha = 1.3$ by Li et al., and $\alpha = 1$ by Fang et al.), where the increasing flame diameter D_f and flame temperature T_f combined with the decreasing surface temperature T_s under low pressure finally lead to the exponent factor α being less than 2.

In the study of Zarzecki et al. [42], D_f was briefly set as a constant equaling the burner diameter, which is not veritable for the air pressure influence. A rough prediction on flame diameter can be derived from the study on laboratory-scale laminar diffusion flames [43], where $D_f \underset{(D,\dot{m}'')}{\sim} P^{-0.5}$ (the symbol $\underset{(D,\dot{m}'')}{\sim}$ denotes the proportional relationship for the same burner size D, and fuel flow rate $\dot{m}''$). Thus,

$$L_m \underset{(D,\dot{m}'')}{\sim} P^{-0.5} \tag{8}$$

Besides, flame volume V_f equals

$$V_f = \pi(D_f^2/4)z_f \underset{(D,\dot{m}'')}{\sim} P^{-1.4} \tag{9}$$

Finally, the radiant fraction at a fixed burner size and fuel flow rate can be expressed as,

$$X_r \underset{(D,\dot{m}'')}{\sim} \dot{Q}_r \underset{(D,\dot{m}'')}{\sim} P^{0.6}T_f^4 \tag{10}$$

Previous studies indicated that a slightly higher flame temperature aroused by the decreasing pressure [6,35,44], then the counteraction of T_f and P finally leads to the little decrease in X_r under low pressure [4]. However, in most situations, e.g. in the analysis of fire plume, flame temperature and radiant fraction can be rationally regarded as a constant for their fairly week dependence on pressure.

3.4. Axial temperature distribution

Axial temperature distribution is usually scaled by z/z^*, where $z^* = [Q/(\rho_\infty c_p T_\infty \sqrt{g})]^{2/5}$ is introduced as a characteristic length in fire scaling [18,27,45]. Under normal pressure, z^* is generally expressed in a simplified form as $Q^{2/5}$. By aid of the simplified term $Q^{2/5}$, three explicit regions of the fire plume are delineated by McCaffrey [11] as flame region ($z/Q^{2/5} < 0.08$), intermittent region ($z/Q^{2/5}$: 0.08–0.2) and plume region ($z/Q^{2/5} > 0.2$), with the temperature rise $T - T_\infty$ proportional to $(z/Q^{2/5})^0$, $(z/Q^{2/5})^{-1}$ and $(z/Q^{2/5})^{-5/3}$, respectively in these regions. To include the pressure effect in the analysis of axial temperature, the characteristic length should be further suggested as $z^* \sim (Q/P)^{2/5}$, and then the averaged temperature rise $T - T_\infty$ along the burner axis can be scaled by $z(P/Q)^{2/5}$ (see Fig. 8).

Derived from the analysis of mass and heat transfer, Quintiere [18] and Heskestad [15] concluded the following empirical expressions, which are respectively given for flame and plume regions,

Quintiere relation for flame region:

$$\frac{T - T_\infty}{T_\infty} = C_{T,1}(1 - X_r)\frac{H_c/r}{c_p T_\infty} \tag{11}$$

Quintiere relation for far-field plume region:

$$\frac{T - T_\infty}{T_\infty} = C_{T,2}(1 - X_r)^{2/3}\left(\frac{z}{z^*}\right)^{-5/3} \tag{12}$$

Heskestad relation for plume region (criterion: $T - T_\infty \leqslant 500\ ^\circ\text{C}$ or $z \geqslant z_f$)

$$\frac{T - T_\infty}{T_\infty} = C'_{T,2}(1 - X_r)^{2/3}\left(\frac{z + z_0}{z^{*2/5}}\right)^{-5/3} \tag{13}$$

Here, $X_r = 0.4$ for n-Heptane fires [46–48]. The constant $C_{T,1}$ varies from 0.347 to 0.427 [18], which depends on the accuracy of the flame temperature measurements, $C_{T,2} = 10.58$ [18], and $C'_{T,2} = 9.1$ [15]. The concept of a virtual origin, $z_0 = 1.02D - 1.38(Q^*)^{2/5}D$, was introduced by Heskestad [15] for plume region that is not far enough. Eq. (13) with the modification of virtual origin even agrees well in the intermittent region [15]. The application of Eq. (13) is limited to two empirical criteria, i.e. criterion I: $T - T_\infty \leqslant 500\ ^\circ\text{C}$ or criterion II: $z \geqslant z_f$. For far-field plume region, z_0 can be ignored to transform Eq. (13) into Eq. (12) [28].

Fig. 9 shows the fitting results based on the correlations by Quintiere [18], where the three regions of fire plume can be well indentified with the values of $C_{T,1}$ and $C_{T,2}$ fitted using Eqs. (11) and (12) are 0.374 and 9.04. The fitted $C_{T,2} = 9.04$ is lower than the value 10.58 suggested in [18,28], which is probably because the simplified assumption of point source is not suitable for finite real fire.

Based on an alternative form of Eq. (13) [28,45], Fig. 9 can be easily converted into Fig. 10, where the linear fit is only implemented in the plume region as described by Heskestad [15]. The x-axial and y-axial variables show the strong linear relations with Pearson correlation coefficients (R) of 0.97 and 0.94 for the data

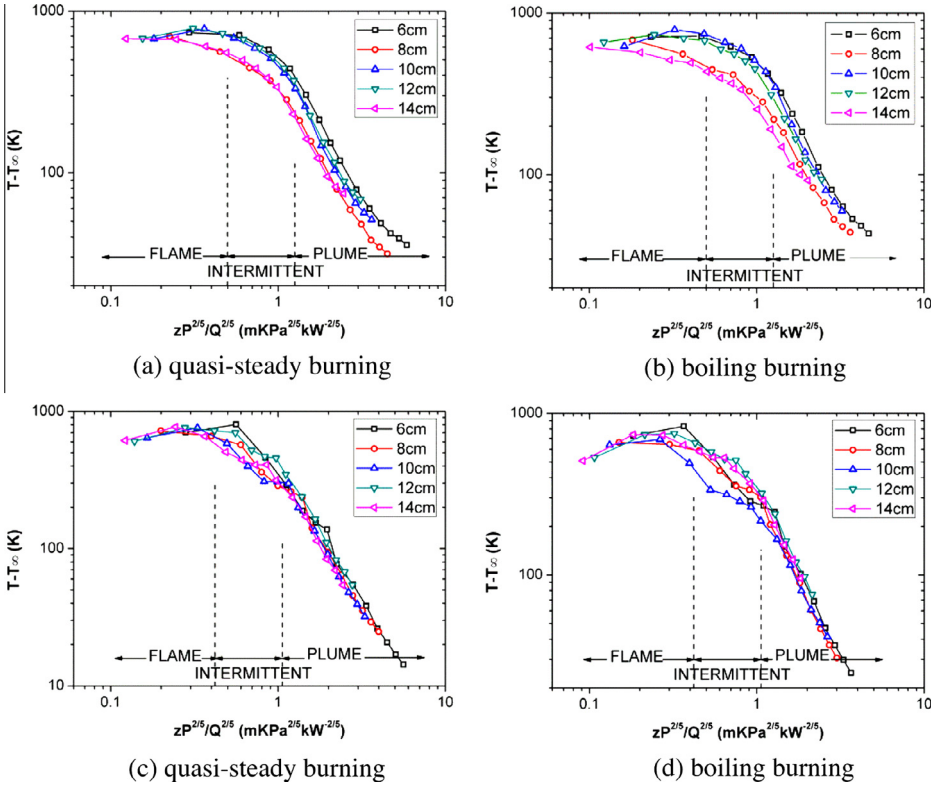

Fig. 8. Averaged axial temperature rise scaled by $zP^{2/5}/Q^{2/5}$ (a) and (b) in Hefei, (c) and (d) in Lhasa.

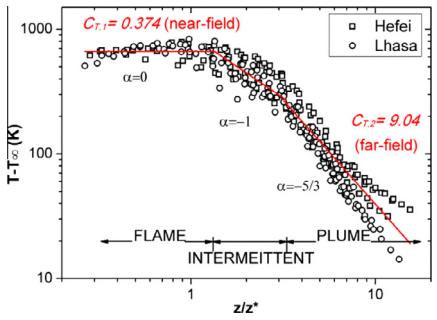

Fig. 9. Averaged axial temperature rise correlated with axial height using Quintiere relations [18].

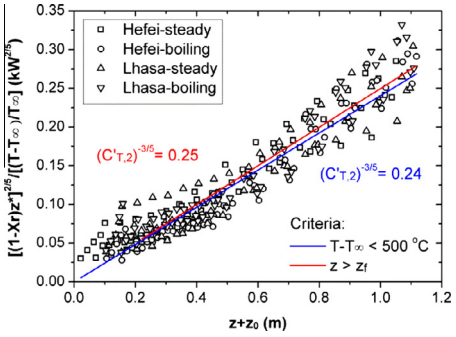

Fig. 10. Averaged plume temperature rise correlated with axial height using the Heskestad relation [15].

partitioned by criteria I and II. Furthermore, the fitted values of $C'_{T,2}$ indicate extremely small errors in the linear fits where the adjusted coefficients of determination $\overline{R}^2 > 0.99$. $C'_{T,2}$ is respectively fitted as 10.8 and 10.1, which are slightly higher than the empirical value of 9.1 obtained at normal pressure [15]. The parameter $C'_{T,2}$ obtained under the criterion directly defined using flame height $z \geqslant z_f$ is closer with the previous theoretical result. Under lower pressure, the flame is stretched and the plume temperature increases at the same height, thus both the criteria define a farther initial location for the plume region.

The averaged temperature rises in the flame region for quasi-steady and boiling burning stages in Hefei were 678 and 638 °C, slightly lower than those in Lhasa, i.e. 692 and 665 °C. The observation of higher flame temperature in Lhasa is consistent with previous studies [2,4,6], which can be explained by the decreasing radiative heat loss [35,44] and weaker ambient air entrainment cooling for lower air density [2]. There is less soot loading in flames when the pressure is reduced, while the ensemble flame volume or the mean beam length becomes larger with decreasing pressure. These two factors are competing with each other as far as radiative heat loss from the flame is concerned. However, it has been experimentally observed [35,44] that radiative heat loss from the flame is reduced with decreasing pressure, and generally leads to a slight decreasing X_r in Lhasa as discussed in Section 3.3. Consequently, the temperature rise increases with the decreasing of pressure due mainly to the reduced soot level.

The far-field plume temperature can be further transformed from Eq. (12) to a function as $(T-T_\infty)/T_\infty \sim (z/D)^{-5/3}(Q^*)^{2/3} \sim (z/z_f)^{-5/3} \underset{D}{\sim} P^{2(\alpha-1)/3}$, which indicates that plume temperature increases under low pressure. The flame stretching (or increasing in flame height z_f) under low air pressure leads to the relative downward shift of temperature measuring points in the flame. Under low pressure, the plume temperature measurements at the same height actually shift closer to the flame envelope, i.e. the location of stoichiometric mixture fraction, and correspondingly the measured plume temperature increases towards the flame temperature.

4. Conclusion

The effects of low air pressure on fire plume in the quasi-steady burning stage and the boiling–burning stage were analyzed based on the experimental measurements on mass burning rate, flame height, and axial temperature distribution. The classical theories on fire plume were adopted to establish a unified analysis.

From the analysis of pressure effect on flame heat feedback, the burning intensity is concluded as a power function of pressure $\dot{m}'' \underset{D}{\sim} P^{\alpha}$, where the power α varies for different heat feedback modes: $\alpha < 0$ for conductively dominated mode, $0 < \alpha < 2/3$ for transition mode, and $\alpha \geqslant 2/3$ for convectively dominated mode. As the pool dimension increases, the power α increases gradually. The burning in the boiling stage is more prone to be conductively dominated.

To characterize fire plumes under different pressures, the dimensionless heat release rate and characteristic length were modified as $Q^* \sim Q/PD^{5/2}$ and $z^* \sim (Q/P)^{2/5}$ by adding a pressure term into the previously-used $Q^* \sim Q/D^{5/2}$ and $z^* \sim Q^{2/5}$ for standard pressure cases. The dimensionless heat release rate for the same pan size is related to the pressure by $Q^* \underset{D}{\sim} P^{(\alpha-1)}$, and correspondingly the flame height is related to the pressure by $z_f \underset{D}{\sim} P^{0.4(\alpha-1)}$. The power $\alpha < 1$ indicates that flame height increases under lower pressure, as validated by the averaged visible flame heights obtained from the flame images in Hefei and Lhasa.

The combined effects of expanded flame volume and reduced soot yield under lower pressure lead to a decreased radiative heat loss, which increases the flame temperature. The relationships between flame temperature and radiant fraction are complex and coupled. Generally, X_r and T_f are weekly dependent on pressure, and both can be considered as constants in most situations. Modifications of model constants for low-pressure fire plumes were proposed to correlate the measured axial temperature with the axial height in the plume region by the Quintiere and Heskestad relations. The correlation $(T-T_\infty)/T_\infty \sim (z/z_f)^{-5/3} \underset{D}{\sim} P^{2(\alpha-1)/3}$ indicates that the plume temperature increases under lower pressure. The flame stretching under low pressure leads to the shrink of relative height (z/z_f), which means that the measurement at the fixed height is closer to the stoichiometric mixture fraction and thus the measured plume temperature increases towards the flame temperature.

Acknowledgment

The work described in this paper was supported by Key Program of National Natural Science Foundation of China (No. 51376172) and a Grant from the Research Grant Council of the Hong Kong Special Administrative Region [Project No. CityU 122612]. The authors deeply appreciate the supports.

References

[1] D. Wieser, P. Jauch, U. Willi, The influence of high altitude on fire detector test fires, Fire Safety J. 29 (2) (1997) 195–204.
[2] Z. Li, Y. He, H. Zhang, J. Wang, Combustion characteristics of n-heptane and wood crib fires at different altitudes, Proc. Combust. Inst. 32 (2) (2009) 2481–2488.
[3] X. Hu, Y. He, Z. Li, J. Wang, Combustion characteristics of n-heptane at high altitudes, Proc. Combust. Inst. 33 (2) (2011) 2607–2615.
[4] J. Fang, R. Tu, J. Guan, J. Wang, Y. Zhang, Influence of low air pressure on combustion characteristics and flame pulsation frequency of pool fires, Fuel 90 (8) (2011) 2760–2766.

[5] J. Fang, C. Yu, R. Tu, L. Qiao, Y. Zhang, J. Wang, The influence of low atmospheric pressure on carbon monoxide of n-heptane pool fires, J. Hazard. Mater. 154 (1) (2008) 476–483.
[6] R. Tu, J. Fang, Y. Zhang, J. Zhang, Y. Zeng, Effects of low air pressure on radiation-controlled rectangular ethanol and n-heptane pool fires, Proc. Combust. Inst. 34 (2) (2012) 2591–2598.
[7] J.W. Reinhardt, Minimum Performance Standard for Aircraft Cargo Compartment Halon Replacement Fire Suppression Systems, Federal Aviation Administration, Springfield, Virginia, 2005.
[8] Y. Niu, Y. He, X. Hu, D. Zhou, C.H. Lin, J. Yin, W. Yao, J. Wang, Experimental study of burning rates of cardboard box fires near sea level and at high altitude, Proc. Combust. Inst. 34 (2) (2012) 2565–2573.
[9] W. Yao, X. Hu, J. Rong, J. Wang, H. Zhang, Experimental study of large-scale fire behavior under low pressure at high altitude, J. Fire Sci. 31 (4) (2013).
[10] P.H. Thomas, C.T. Webster, M.M. Raftery, Some experiments on buoyant diffusion flames, Combust. Flame 5 (4) (1961) 359–367.
[11] B.J. McCaffrey, Purely Buoyant Diffusion Flames: Some Experimental Results, National Bureau of Standards, 1979.
[12] E.E. Zukoski, Fluid dynamic aspects of room fires, in: Fire Safety Science – Proceedings of the First International Symposium, Fire, Safety Science, 1986, pp. 1–30.
[13] E.E. Zukoski, B.M. Cetegen, T. Kubota, Visible structure of buoyant diffusion flames, Proc. Combust Inst. 20 (1) (1985) 361–366.
[14] G. Heskestad, Luminous heights of turbulent diffusion flames, Fire Safety J. 5 (2) (1983) 103–108.
[15] G. Heskestad, Virtual origins of fire plumes, Fire Safety J. 5 (2) (1983) 109–114.
[16] G. Heskestad, Fire plume air entrainment according to two competing assumptions, Proc. Combust Inst. 21 (1) (1988) 111–120.
[17] G. Heskestad, A reduced-scale mass fire experiment, Combust. Flame 83 (3–4) (1991) 293–301.
[18] J.G. Quintiere, B.S. Grove, A unified analysis for fire plumes, Proc. Combust. Inst. 27 (2) (1998) 2757–2766.
[19] J.S. Yin, W. Yao, Q.Y. Liu, Z.H. Zhou, N. Wu, H. Zhang, C.H. Lin, T. Wu, O.C. Meier, Experimental study of n-heptane pool fire behavior in an altitude chamber, Int. J. Heat Mass Transfer 62 (1) (2013) 543–552.
[20] M. Luo, Y. He, V. Beck, Application of field model and two-zone model to flashover fires in a full-scale multi-room single level building, Fire Safety J. 29 (1) (1997) 1–25.
[21] Q. Kang, S. Lu, B. Chen, Experimental study on burning rate of small scale heptane pool fires, Chin. Sci. Bull. 55 (10) (2010) 973–979.
[22] J.M. Chatris, J. Quintela, J. Folch, E. Planas, J. Arnaldos, J. Casal, Experimental study of burning rate in hydrocarbon pool fires, Combust. Flame 126 (1–2) (2001) 1373–1383.
[23] D. Drysdale, An Introduction to Fire Dynamics, John Wiley and Sons, New York, 1998.
[24] A.M. Kanury, Modeling of pool fires with a variety of polymers, Proc. Combust. Inst. 15 (1) (1975) 193–202.
[25] B.M. Cetegen, T.A. Ahmed, Experiments on the periodic instability of buoyant plumes and pool fires, Combust. Flame 93 (1–2) (1993) 157–184.
[26] M. Yang, Y. He, H. Li, J. Wang, Combustion of laminar non-premixed acetylene jet at two different altitudes, Combust. Sci. Technol. 184 (12) (2012) 1950–1969.
[27] G. Heskestad, Fire plumes, flame height, and air entrainment, in: P.J. DiNenno (Ed.), SFPE Handbook of Fire Protection Engineering, third ed., 2002, pp. 1–17.
[28] J.G. Quintiere, Fundamentals in Fire Phenomena, John Wiley & Sons, LTD, 2006.
[29] J. Benesty, J. Chen, Y. Huang, I. Cohen, Pearson correlation coefficient, in: Noise Reduction in Speech Processing, Springer, Berlin Heidelberg, 2009, pp. 1–4.
[30] M. Kumar, V.K. Srivastava, Pitman nearness and concentration probability comparisons of the sample coefficient of determination and its adjusted version in linear regression models, Commun. Stat. – Theory Methods 33 (7) (2004) 1629–1641.
[31] J.G. Liao, D. McGee, Adjusted coefficients of determination for logistic regression, Am. Stat. 57 (3) (2003) 161–165.
[32] R. Sivaramakrishnan, A. Comandini, R.S. Tranter, K. Brezinsky, S.G. Davis, H. Wang, Combustion of CO/H_2 mixtures at elevated pressures, Proc. Combust. Inst. 31 (1) (2007) 429–437.
[33] T. Beji, J.P. Zhang, W. Yao, M. Delichatsios, A novel soot model for fires: validation in a laminar non-premixed flame, Combust. Flame 158 (2) (2011) 281–290.
[34] A.E. Karataş, Ö.L. Gülder, Soot formation in high pressure laminar diffusion flames, Prog. Energy Combust. 38 (6) (2012) 818–845.
[35] A.E. Karatas, G. Intasopa, O.L. Guelder, Sooting behaviour of n-heptane laminar diffusion flames at high pressures, Combust. Flame 160 (9) (2013) 1650–1656.
[36] W. Yao, J. Zhang, A. Nadjai, T. Beji, M.A. Delichatsios, A global soot model developed for fires: validation in laminar flames and application in turbulent pool fires, Fire Safety J. 46 (7) (2011) 371–387.
[37] W. Yao, J. Zhang, A. Nadjai, T. Beji, M. Delichatsios, Development and validation of a global soot model in turbulent jet flames, Combust. Sci. Technol. 184 (5) (2012) 717–733.
[38] W. Yao, J. Ying, X. Hu, J. Wang, H. Zhang, Numerical modeling of liquid n-heptane pool fires based on heat feedback equilibrium, in: The 9th Asia-Oceania Symposium on Fire Science and Technology, Hefei, 2012.
[39] J.L. De Ris, P.K. Wu, G. Heskestad, Radiation fire modeling, Proc. Combust. Inst. 28 (2) (2000) 2751–2759.
[40] J. De Ris, Fire radiation – a review, Proc. Combust. Inst. 17 (1) (1979) 1003–1016.
[41] L. Orloff, J. De Ris, Froude modeling of pool fires, Proc. Combust. Inst. 19 (1) (1982) 885–895.
[42] M. Zarzecki, J.G. Quintiere, R.E. Lyon, T. Rossmann, F.J. Diez, The effect of pressure and oxygen concentration on the combustion of PMMA, Combust. Flame 160 (8) (2013) 1519–1530.
[43] L.L. McCrain, W.L. Roberts, Measurements of the soot volume field in laminar diffusion flames at elevated pressures, Combust. Flame 140 (1–2) (2005) 60–69.
[44] D. Bento, K. Thomson, O. Gulder, Soot formation and temperature field structure in laminar propane–air diffusion flames at elevated pressures, Combust. Flame 145 (4) (2006) 765–778.
[45] G. Cox, R. Chitty, Some source-dependent effects of unbounded fires, Combust. Flame 60 (3) (1985) 219–232.
[46] A. Tewarson, Combustion efficiency and its radiative component, Fire Safety J. 39 (2) (2004) 131–141.
[47] A. Tewarson, J.L. Lee, R.F. Pion, The influence of oxygen concentration on fuel parameters for fire modeling, Proc. Combust Inst. 18 (1) (1981) 563–570.
[48] J.C. Yang, A. Hamins, T. Kashiwagi, Estimate of the effect of scale on radiative heat loss fraction and combustion efficiency, Combust. Sci. Technol. 96 (1–3) (1994) 183–188.